Article

Pressing and Sintering of Titanium Aluminide Powder after Ball Milling in Silane-Doped Atmosphere

Bernd-Arno Behrens [1], Kai Brunotte [1], Julius Peddinghaus [1], Jonathan Ursinus [1], Sebastian Döring [1,*], Wolfgang Maus-Friedrichs [2], René Gustus [2] and Maik Szafarska [2,*]

[1] Institut für Umformtechnik und Umformmaschinen, Leibniz Universität Hannover, 30823 Garbsen, Germany; behrens@ifum.uni-hannover.de (B.-A.B.); brunotte@ifum.uni-hannover.de (K.B.); peddinghaus@ifum.uni-hannover.de (J.P.); ursinus@ifum.uni-hannover.de (J.U.)

[2] Clausthaler Zentrum für Materialtechnik, Technische Universität Clausthal, 38678 Clausthal Zellerfeld, Germany; wolfgang.maus-friedrichs@tu-clausthal.de (W.M.-F.); rene.gustus@tu-clausthal.de (R.G.)

[*] Correspondence: s.doering@ifum.uni-hannover.de (S.D.); maik.szafarska@tu-clausthal.de (M.S.); Tel.: +49-(0)5117-624106 (S.D.); +49-(0)5323-723374 (M.S.)

Abstract: Due to the high specific surface area of titanium aluminide powders, significant and unavoidable surface oxidation takes place during processing. The resulting oxides disrupt the conventional powder metallurgical process route (pressing and sintering) by reducing the green strength and sintered properties. Oxide-free particle surfaces offer the potential to significantly increase particle bond strength and enable the processing of difficult-to-press material powders. In this work, the effect of milling titanium aluminide powder in a silane-doped atmosphere on the component properties after pressing and the subsequent sintering was investigated. Ball milling was used to break up the oxide layers and create bare metal surfaces on the particles. With the help of silane-doped inert gas, the oxygen partial pressure was greatly reduced during processing. It was investigated whether oxide-free surfaces could be produced and maintained by milling in silane-doped atmospheres. Furthermore, the resulting material properties after pressing and sintering were analysed using density measurements, hardness tests, EDX measurements, and micrographs. It was concluded that ball milling in a silane-doped atmosphere produces and maintains oxide-free particle surfaces. These oxide-free surfaces and smaller particle sizes improve the component properties after pressing and sintering.

Keywords: die pressing and sintering; powder metallurgical process; titanium aluminide powder

1. Introduction

Titanium aluminides (TiAl) are intermetallic materials, and γ-alloys, in particular, offer great application potential in automotive and aerospace applications [1]. Whenever good creep resistance combined with low density at high operating temperatures is required, TiAl alloys with a density of only 3.9–4.2 g/cm^3 represent a lighter alternative to titanium or nickel-based alloys. The properties of TiAl materials essentially depend on the microstructure, which, in turn, is determined by the alloy and the manufacturing and processing methods [2].

In order to improve the chemical and microstructural homogeneity compared to cast-starting material, TiAl alloys are predominantly processed powder-metallurgically [3]. After the starting powder has been produced by inert gas atomisation, it is solidified by hot isostatic pressing (HIP) [4]. Subsequently, it is shaped by isothermal forging [5]. Alternatively, the component geometry is created directly from powder using the modified sintering processes, field-assisted sintering (FAST) [6].

HIP, isothermal forging, and FAST are demanding processes with a high technical complexity. In contrast, die pressing and sintering have established themselves as a

cost-effective and productive near-net-shape process for many other metallic powder materials [7]. However, the low ductility of the particles poses a challenge when processing TiAl powder via the conventional process route. In addition, the oxide layers present make processing more difficult, which are of secondary importance in the processes established to date (e.g., FAST), as the oxide layers are broken up during the process there [8,9].

Titanium aluminides have a high affinity for oxygen, which influences the microstructure development and, thus, the technological properties [10]. Interstitially resolved oxygen leads to an increased strain hardening of the powder, which reduces the compressibility during pressing and only weak surface contacts can be built up [11]. Furthermore, oxide layers consisting of titanium and aluminium oxides, as well as mixed oxides, build on the particle surfaces [12]. In die pressing, a strong bond is to be produced by cold welding the powder particles [13]. However, the existing oxide layers hinder the interlocking and the cold welding [14]. This leads to a reduction in compressibility and, thus, to reduced green strength [15]. During sintering, the oxide layers act as a diffusion barrier and, therefore, cause high porosities. They also reduce the thermal conductivity and the sinterability of powders [16]. This results in the formation of inhomogeneities in the microstructure [17].

TiAl powders react with oxygen when exposed to air, even at ambient temperatures, and should be processed under inert gas atmospheres to prevent an undesirable increase in the oxygen content of the powder particles [18]. However, in most inert gas atmospheres such as argon, the residual oxygen content is too high and must be reduced to inhibit oxidation [19].

This is where the present study comes in by using silane-doped argon as the process atmosphere. Monosilane (SiH_4) reacts with the residual oxygen of argon 5.0, which is about 2 ppm_v, and, thus, enables very low oxygen concentrations well below 10^{-20} ppm_v [20,21]. It is investigated whether and under which conditions a qualification of the conventional powder metallurgical process route (pressing and sintering) for titanium aluminium materials can be achieved by processing in this extremely low-oxygen atmosphere. It will be investigated whether the existing oxide layers can be broken up and preserved by ball milling. In addition, the influence of the grinding, the atmosphere, and the applied parameters on the component properties after pressing and sintering will be analysed.

2. Materials and Methods

The investigation was conducted on TiAl powder belonging to the GE48 alloy (with the following composition in wt.%: 59.60% Ti, 33.00% Al, 2.60% Cr, and 4.80% Nb). This powder was produced through inert gas atomisation using argon and possesses a spherical morphology. The D90 value, representing the maximum particle size where 90% of the initial powder volume is encompassed, was measured at 134 μm. Additionally, the powder exhibited an oxygen concentration of 909 ppm_w. The material demonstrated density of 3.97 g/cm^3 (Gesellschaft für Elektrometallurgie, Nuremberg, Germany).

In a glovebox (GS Glovebox Systemtechnik GmbH, Malsch, Germany), the silane-doped atmosphere was generated. It was pre-purged with argon 5.0 (purity $\geq$ 99.99%). Afterwards, rinsing was carried out with argon/monosilane (99% Ar/1% SiH4), so that the residual oxygen contained in the argon 5.0 reacts with the monosilane to form silicon dioxide and the oxygen concentration is consequently reduced. Hydrogen is also produced in the process.

$$SiH_4 \text{ (g)} + O_2 \text{ (g)} \rightarrow SiO_2 \text{ (s)} + 2H_2 \text{ (g)} \tag{1}$$
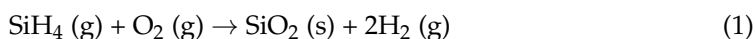
The regulation of argon and argon/silane was realised via corresponding flow meters, which allow the control of the atmosphere especially in the transient start-up phase. The oxygen partial pressure was measured via a sensor box with lambda probe (L-Probe EM2020, Mesa GmbH, Schmalkalden, Germany) and adjusted to below 10^{-18} ppm_v during the experiments.

Under this atmosphere, the GE48 powder was filled into the ball-grinding containers (FRITSCH GmbH, Idar-Oberstein, Germany, 250 mL, hardened steel DIN EN 10027-1 X105CrMo17). Two containers were filled with 40 g of powder each and 345 g of milled

steel balls (X105CrMo17) with a diameter of 10 mm and sealed gas-tight so that the oxygen partial pressure was also below 10^{-18} ppm$_v$ during the entire grinding process. The weight ratio of the steel balls and powder was chosen according to Murty et al. [22]. To minimise agglomeration due to cold welding, 12 drops of toluene (C_7H_8) were added [6]. The ball-milling process was carried out with a Pulverisette 5/4 planetary ball mill (FRITSCH GmbH, Idar-Oberstein, Germany) at a speed of 300 1/min. Following Shengguan et al., where a relative density of 96% was achieved after sintering by milling TiAl powder, an effective milling time of 5 h was set with an interruption of 4 min cyclically after every 3 min of active ball milling [23]. To avoid excessive heating of the milling vessels and to maintain stable process conditions, a further break of 10 min was taken after every 5 cycles.

After ball milling, the containers were reopened for further processing in the glove box with the oxygen-free atmosphere described above. The atmospheric and compacting conditions were varied to detect the effects of atmospheric conditions on this conventional powder metallurgical processing route. Table 1 shows an overview of the different sample variants. The variants XHV6 and XHV8 were compacted without contact with ambient air at two different compaction pressures. For further tests, the compression pressure was kept constant (800 MPa). The V8 variant was subjected to vacuum drying in the airlock of the glove box in a silane-doped atmosphere in order to evaporate any toluene residue. In addition to creating the desired oxide-free surface areas, the milling process also reduces the particle size of the powder. In order to assess the effect of the oxide surface conditions isolated from the effect of the particle size, additional reference samples were created with powder, exposed to ambient air after milling (L85 and L840). Variant REF represents the untreated reference with the particle size and shape before milling. Compaction to green bodies of 7 g and 20 mm diameter was carried out by one-sided pressing with a manually driven hydraulic press (MSE Teknoloji. Osb/Gebze/Kocaeli, Turkey) in the glove box.

Table 1. Processing variants of the GE48 powder.

Designation	Pressure in MPa	Treatment
XHV6	600	Ball-milled
XHV8	800	Ball-milled
V8	800	Vacuum drying
L85	800	5 min in air
L840	800	40 min in air
REF	800	Untreated

Later, all green compacts were sintered in a hot tube furnace (Thermconcept ROC, Bremen, Germany) at 1300 °C for 60 min. The chosen temperature for the sintering process is based on previous FAST experiments that have successfully produced a desirable lamellar microstructure at this specific temperature [24]. Via a cooled flange, the samples are transported from the glove box directly to the oven. The oven is supplied with an oxygen-free atmosphere through a fan, effectively maintaining the oxygen partial pressure during sintering below an impressive 10^{-18} ppm$_v$ (as depicted in Figure 1).

For each process step, an analysis of the powder or sample was carried out. In order to investigate the influence of the particle size on the microstructure after ball milling, the particle size distribution of the milled and unmilled powder was determined. The measurement was carried out with a laser diffraction measuring system (HELOS, Sympatec, Clausthal-Zellerfeld, Germany). With the measuring system, the particle size can be determined in a measuring range from 0.1 μm to 8.750 mm. The characterisation of the elemental composition as well as the chemical state of the particle surface was carried out by X-ray photoelectron spectroscopy (XPS) with an information depth of about 10 nm in a modified UHV (ultra-high vacuum) apparatus (VG ESCALAB MKII, Manufacturer: VG Scientific (now: Thermo Scientific), Waltham, MA, USA) with a base pressure of 2×10^{-10} mbar. Between the ball-milling process and the measurement, the TiAl powder milled in a silane-doped atmosphere had no contact with the surrounding atmosphere due

to a special transport system [25]. With the help of XPS measurement, the newly formed surfaces of the powder particles were examined with regard to oxidation. In XPS, X-rays are focused on the sample surface, where electrons are emitted due to the photoelectric effect. These photoelectrons have characteristic kinetic energies that correspond to the binding energy of their respective original orbital, which, in turn, is also influenced by the chemical state of the element involved. With the help of a hemispherical electron energy analyser, the electrons can be sorted according to their energy, which enables the presentation of a photoelectron spectrum. Non-monochromatic Al-Kα radiation (1486.6 eV) was used for XPS measurements generated in an XR40B X-ray source from PREVAC GmbH (Berlin, Germany). The electron-pass energy was set to 100 eV for survey spectra and to 20 eV for detail spectra. Spectral analysis was performed using CASAXPS software (Version: 2.3.23PR1.0) from Casa Software Ltd. The spectra were recorded relative to the Fermi level and fitted with the algorithm developed by Levenberg–Marquard, which takes into account photoelectric cross-sections according to Scofield and asymmetry parameters from Reilman et al. [26,27]. Transport and transfer of the oxygen-free powder from the silane-doped argon atmosphere into the UHV chamber was carried out using a validated transfer system described by Gustus et al. [25]. The other powders that were exposed to air were prepared in the conventional way with an airlock and transferred to the XPS instrument.
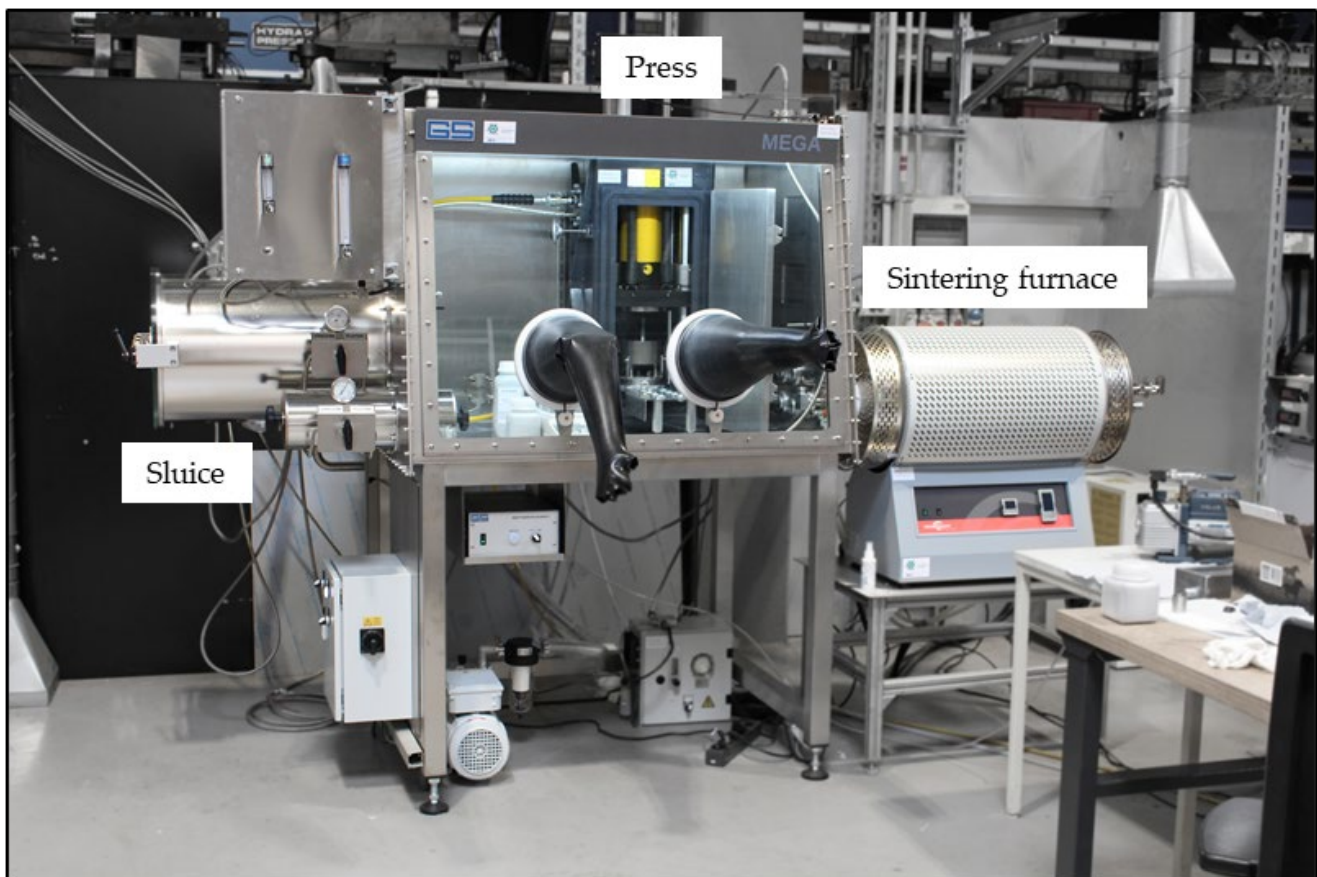

Figure 1. Structure of the glove box with press and sintering furnace.

The green compacts were analysed optically after cold pressing of the prepared powders. These green compacts were examined for cracks and fragmentation. In order to characterise and quantify the mechanical green properties, the splitting tensile strength was determined. This strength test is used for brittle materials [28]. For this purpose, the samples were clamped in a force test rig and radially loaded until the sample broke (see Figure 2).

Figure 2. Test bench when determining the splitting tensile strength.

After sintering, the density of the samples was determined by weighing them in distilled water according to the Archimedes principle with a suitable measuring set-up (Sartorius YDK, Sartorius AG, Göttingen, Germany). Metallographic examinations of the sintered samples (Polyvar MET microscope, Reichert Metek, New York, NY, USA) were carried out on longitudinal sections of the samples without etching and used for qualitative evaluation of the particle composite and the defect structure. EDX examinations (Zeiss Supra 55 VP, Oberkochen, Germany) were carried out for phase determination. The mechanical properties of the sintered specimen were characterised through microhardness measurements. This simplified method was chosen as it allows reproducible comparison between the analysed variants, even with limited specimen dimensions, and correlates directly with the material strength [29]. A Qness Q10A (Mammelzen, Germany) hardness tester was used to determine the hardness of the sintered bodies according to Vickers HV1. The hardness measurements were carried out over the cross-section according to ISO 6507 [30]. Five points were measured in the axial direction and ten points in the radial direction. Subsequently, the average hardness was determined by calculating the mean value from various measuring points. The exposure time during this process was set at 15 s.

3. Results

3.1. Particle Size Distribution

There was a significant reduction in particle size distribution after 5 h of ball milling. The D90 value after milling was 53 μm. This corresponds to a reduction of the particle size to approx. 40%. A detailed representation of the particle size distributions is shown in Figure 3. A narrowing and shift of the particle size spectrum into the range of 0–50 μm can be observed due to the ball milling. As the particle sizes have decreased, the specific surface area has increased. Since no new oxygen is introduced, it can be hypothesised that there are oxide-free surface fractions when the specific surface area has increased. In the following section, the newly formed surfaces were examined with regard to oxidation.
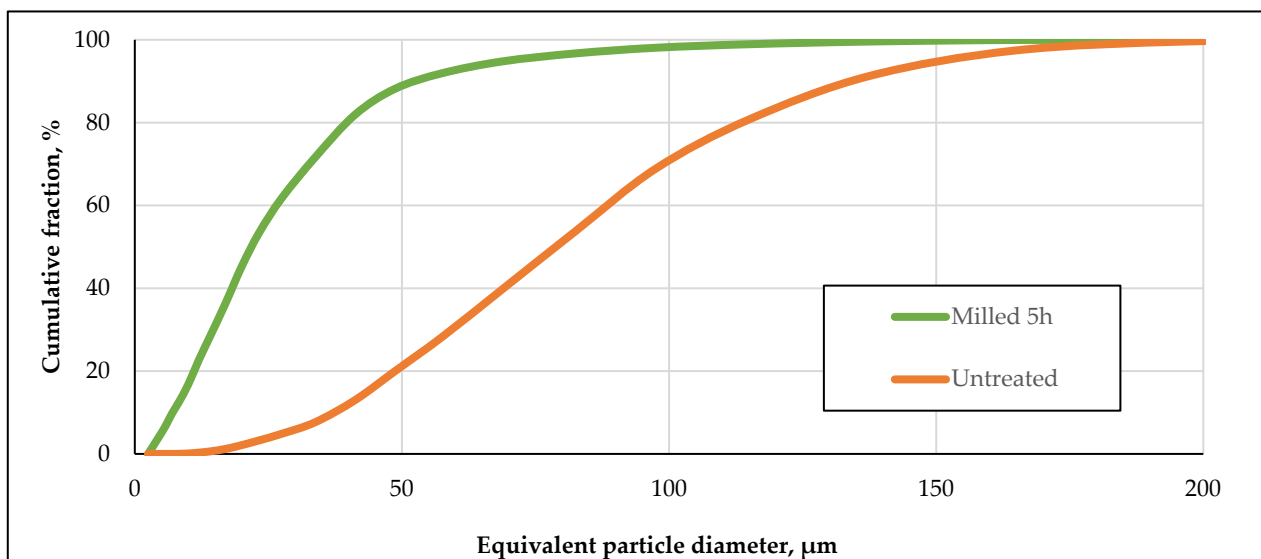
Figure 3. Particle size distribution of GE48 powder before and after milling.

3.2. X-ray Photoelectron Spectroscopy

The O1 spectra on the left side of Figure 4 show that the GEM+OX powder (milled and oxidised, process variants L85 and L840) has the most metal oxides on the particle surface. Most likely, this is due to the increased particle surface area after milling, which tends to re-oxidise in air. The O1 signal is, therefore, composed of the oxide layer broken up by milling and the re-oxidised particle surface. The reference (process variant REF) powder contains a smaller amount of surface metal oxides, where the peak for organic compounds has a higher intensity than that for metal oxides. This trend continues for the OXYGEN-FREE (process variants XHV6, XHV8, and V8) powder, which has the lowest amount of metal oxides in all O1 detail spectra, indicating a decrease in passivating surface oxide layers. Looking at the Ti2p detail spectra on the right side of Figure 3, there is little difference in the chemical state of the titanium species between GEM+OX and the reference sample. This is to be expected as both sample surfaces were exposed to air during fabrication and transport. The largest difference is seen in the Ti2p detail spectrum of the oxygen-free sample. Here, the amount of Ti^{2+} and Ti^{4+} species on the surface is quite similar in contrast to the other two powders. We assign the Ti^{2+}, Ti^{3+}, and Ti^{4+} species to TiO, Ti_2O_3, and TiO_2, respectively, as observed after transporting pure Ti samples in a silane-doped argon atmosphere for extended periods [25]. Silane reacts strongly with oxygen and acts as an oxygen scavenger, but this is not entirely true for water. The reaction between silane and residual water, which remains present in silane-doped argon atmospheres, is kinetically limited [31]. Consequently, the atmosphere is not able to completely prevent the oxidation of titanium, as water can also have an oxidising effect, especially on high-affinity metal surfaces such as titanium and aluminium [32,33]. Lee et al. observed the formation of uniformly distributed Ti^{2+}, Ti^{3+}, and Ti^{4+} species when titanium surfaces were exposed to water, which is consistent with the XPS results discussed in this paper [34]. Overall, however, the Ti2p spectra show significant differences in the chemical composition of the surface of the oxygen-free transported sample compared to the samples transported in air. This suggests that de-oxidation of the GE48 particles has indeed occurred, as it affects the surface chemistry of the powder, even when re-oxidation by residual water molecules in the atmosphere is taken into account.

O1 (left) and Ti2p (right) detail spectra of the GE48 powder samples. Raw data displayed by black lines, orange and blue peaks correspond to either oxygen-containing organic compound (orange) and the metal-oxide species (blue) in the O1s detail spectra. Orange and blue peaks in Ti2p spectra indicate oxidised titanium (orange) and metallic titanium (blue) species respectively. The red-dotted lines show the resulting overall fit.

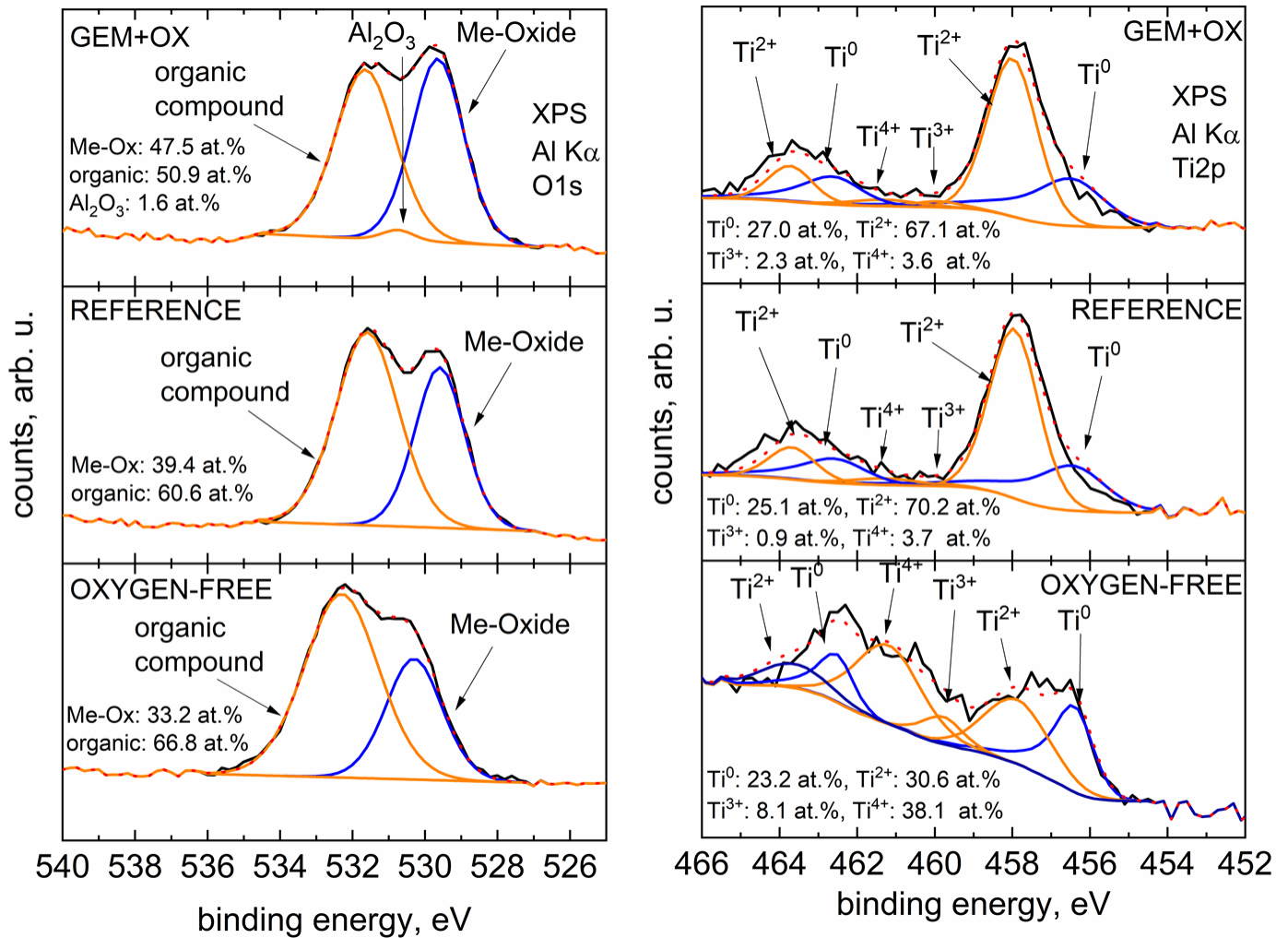Stoichiometry in atomic percent of the species is indicated in the bottom left corner in each detail spectra.

Figure 4. O1 (**left**) and Ti2p (**right**) detail spectra of the GE48 powder samples.

3.3. Pressability

By ball milling the powders, green compacts could be pressed without the need to add any pressing agent or lubricant. However, the variants L85 and L840 exposed to ambient air showed radial cracks and fragmentation after ejection from the pressing tool. Only an unstable bond could be created in the initial powder of the REF sample, which is why the transfer to the sintering furnace already led to a considerable loss of material (see Figure 5).
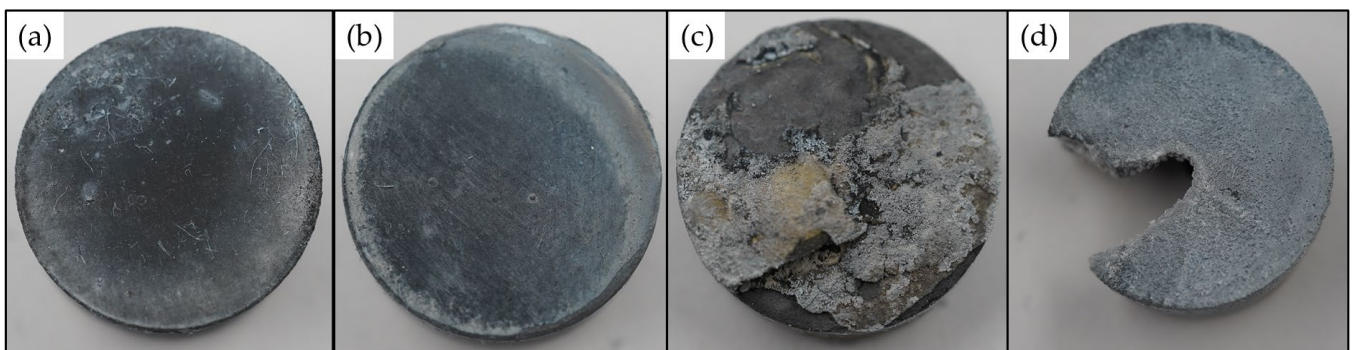

Figure 5. Specimens after pressing: (**a**) XHV8, (**b**) V8, (**c**) L840, and (**d**) REF.

3.4. Splitting Tensile Strength

Figure 6 shows that complete processing in an oxygen-free environment and compacting with a higher pressing pressure leads to a higher tensile splitting strength. Among the variants studied, the XHV8 variant exhibited the highest tensile splitting strength, measuring 1.13 MPa. As the degree of oxidation increased, the strength decreased. A comparison between the XHV6 and XHV8 variants revealed that a lower pressing pressure resulted in a reduced splitting tensile strength. In addition, it can be seen that vacuum drying minimises the splitting tensile strength. However, no specific value could be determined for the REF variant due to its low green strength. This variant disintegrated when inserted.
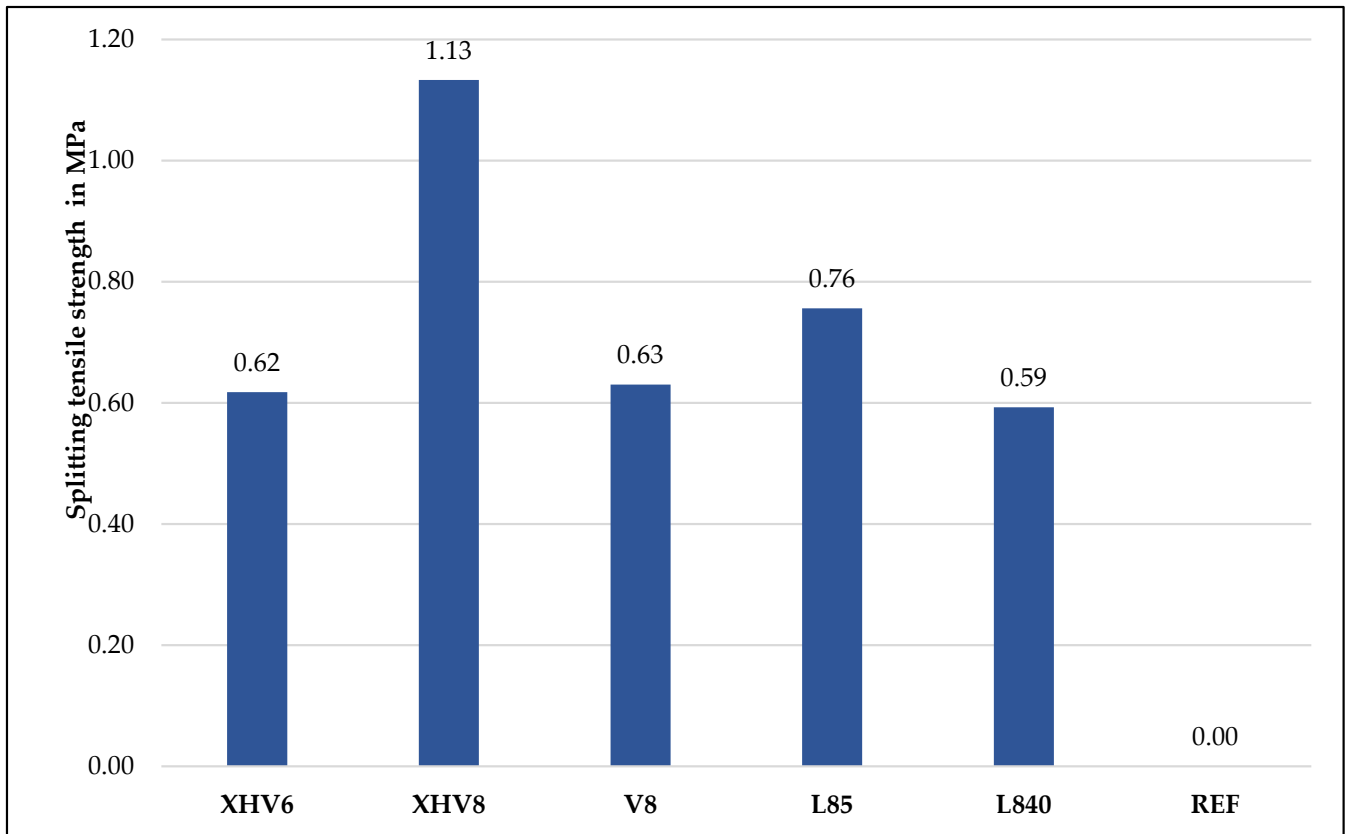

Figure 6. Splitting tensile strength results.

3.5. Density

Table 2 shows the densities of the individual variants. The densities of the ground variants (XHV6, XHV8, V8, L85, and L840) are higher than the density of the unground variant REF (3.42 g/cm^3). Since the densities of the re-oxidised variants (L85 and L840) are higher than those of the XHV8 and V8 variants, no clear influence of the oxygen-free process route can thus be detected. Since all variants have a density lower than 3.97 g/cm^3 (100% rel. density), all samples have porosity. The REF variant has the highest porosity with a relative density of 86%.

Table 2. Sample density.

	XHV6	XHV8	REF	L85	L840	V8
Density	3.69 g/cm^3	3.57 g/cm^3	3.42 g/cm^3	3.65 g/cm^3	3.63 g/cm^3	3.60 g/cm^3
Rel. density	93%	90%	86%	92%	91%	91%

3.6. Microstructure

From the optical microscopic images of the longitudinal sections under polarised light, clear differences between the microstructures of the ground powder and the reference can be seen (Figure 7). First of all, the difference in particle size can be seen. Furthermore, there are inclusions and pores between the particles of the reference sample REF. At the same time, sinter neck formation and recrystallisation across particle boundaries were locally evident. The images of the samples show isolated pores in the microstructure. Furthermore, there are no clear differences between variants without (V8) and with oxygen contact (L840) before pressing. Along the former particle boundaries, bands of dark pits are visible, which can be assigned to the MAX phase Ti_2AlC by EDX measurements (Figure 8).
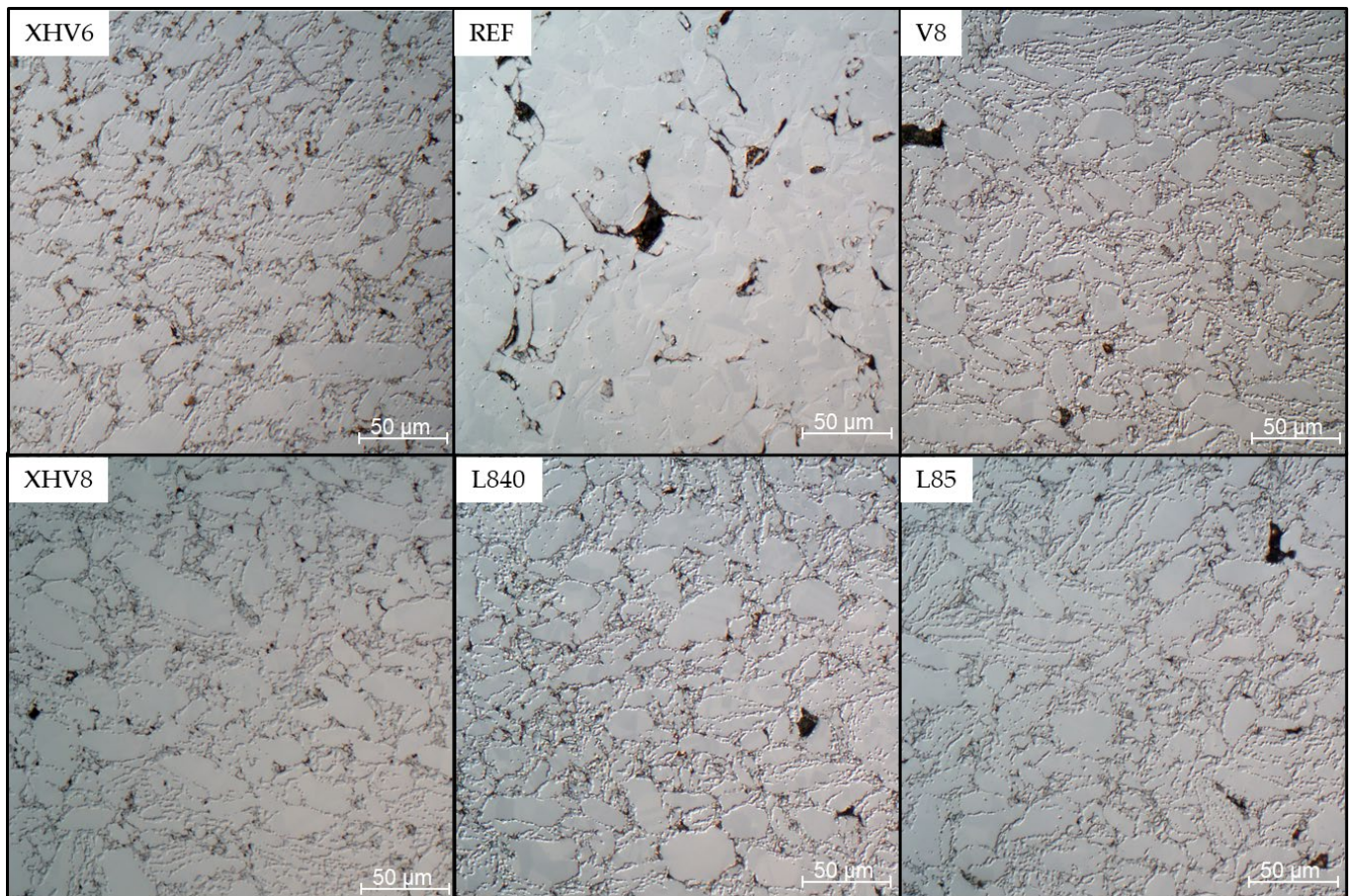

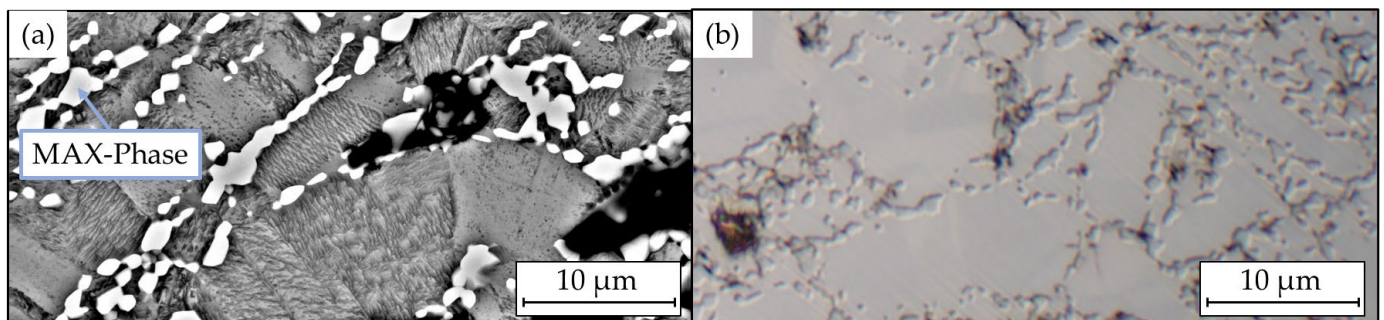**Figure 7.** Images of the central area under polarised light.

Figure 8. MAX phase (**a**) in the microstructure of XHV8 (**b**).

3.7. Hardness

Based on the hardness results in Figure 9, it can be seen that a higher pressing pressure and the milling process lead to a higher hardness. For sample XHV8, there is a 15% increase in hardness compared to REF. The two samples that were exposed to the environment after milling (L85 and L840) show lower hardnesses. As sample L840 was exposed to the environment for a longer period of time, the oxide layer could be more pronounced here. On sample V8, it can be seen that vacuum drying has no influence on the hardness. The difference compared to sample XHV8 is within the standard deviation.
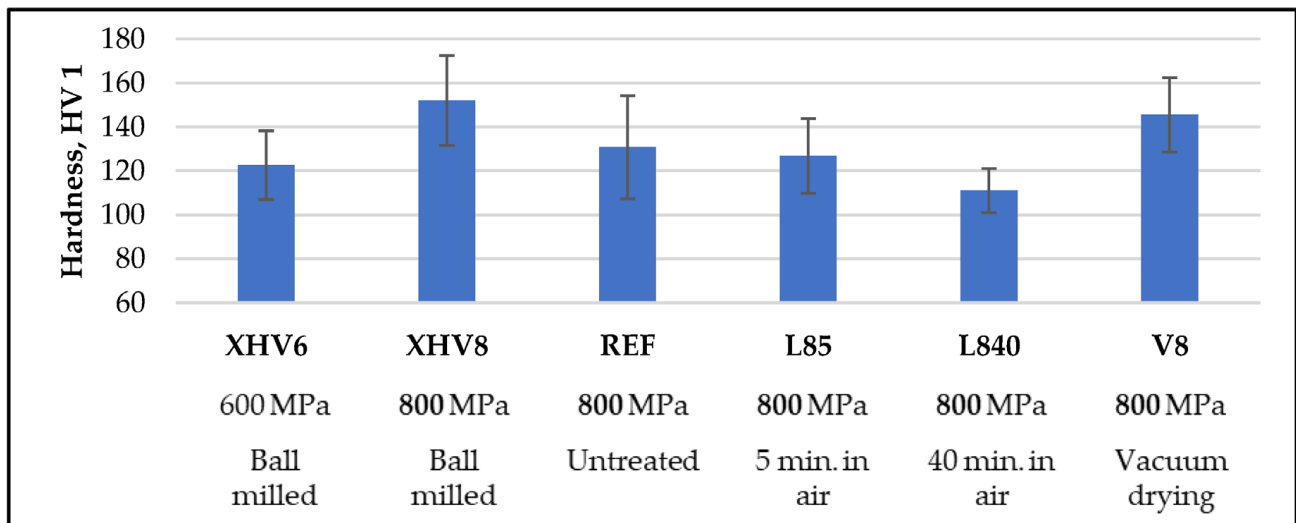

Figure 9. Hardness measurement results according to Vickers.

4. Discussion

The observations and experimental results show that the D90 particle size is reduced from 137 μm to 53 μm during ball milling in a silane-doped atmosphere. In addition, oxide-free particle surfaces are produced and maintained due to the oxygen partial pressure below 10^{-18} ppm$_v$ in the silane-doped atmosphere. The green compacts produced from milled powder exhibit a higher density. This is attributed to the reduction in particle size. The smaller powder particles can fill voids more easily, resulting in a denser component. Therefore, a finer microstructure of the sintered samples is achieved. A clear influence of the oxygen-free environment cannot be seen in the microstructure and density. The EDX measurements showed that the MAX-phase Ti_2AlC formed along the particle boundaries. MAX phases are characterised by a high oxidation resistance in air. In addition, the MAX phases have a better fracture toughness and electrical and thermal conductivity compared to pure TiAl [35,36]. It can be assumed that the carbon input during grinding occurred from the toluene (C_7H_8) used, as this is the only medium apart from the tools used that contains carbon. Decarburisation of the tools is not assumed. The use of ball-milled powder and the consequent reduced particle size leads to a significant improvement in the pressability of the powders (see Figure 5). This indicates the formation of partially oxide-free surfaces on the powder particle. The free surfaces support the cold welding of the particles during pressing, which leads to improved green strength and reduced cracking. This improved green strength was confirmed in the tensile splitting tests. It was shown that a higher pressing pressure leads to a higher splitting tensile strength. Since the two variants L85 and L840 have a lower splitting tensile strength than the XHV8 variant, it can be stated that the oxygen-free processing increases the green strength. Furthermore, it is expected that the bare metal contact of the powder particles favours diffusion during sintering. This is shown by an increase in hardness after sintering from 131 HV1 to 152 HV1 in the oxide-free variants.

The XPS measurements have shown that exposure to air of the powder milled in the silane-doped atmosphere leads to the formation of new oxide layers on the exposed surfaces. Thus, it can be concluded that the ball milling did indeed create oxide-free surfaces which oxidised in reaction with water vapour instead of gaseous oxygen. This finding, together with the experimental results from powder processing highlights the significance of the silane-doped atmosphere. It is elementary to obtain and preserve oxide-free surfaces and to benefit from the oxide-free particle surfaces created by ball milling. Both the processing and the transport to the process steps must take place under the exclusion of oxygen. The effect of ambient air on the oxygen-free milled powder has a significant negative influence on the powder compacts' green strength and, thereby, their processability.

With the chosen sintering parameters, there were no clear effects on density and microstructure after sintering compared to completely oxygen-free processed variants. Since the thermal processes also led to the sintering of the particles in the reference sample without prior ball milling, the barrier effect of the new oxides after milling was apparently overcome during the selected sintering process. The increase in density is, therefore, attributed to the improved pressability of the ground powders. Thus, it can be stated that the ball-milling process breaks up the oxide shards of the TiAl powder and produces oxide-free surfaces. The silane-doped atmosphere inhibits the oxidation of the free surfaces and the oxide-free surfaces are obtained. This allows the TiAl powder to be processed with die pressing and sintering. In the future, the changes in the powder caused by ball milling will be investigated in more detail. In particular, the mechanisms behind oxide layer break-up and the resulting opportunities for process optimisation during sintering will be investigated further.

5. Conclusions

In this study, the influence of grinding, pressing, and sintering in a silane-doped atmosphere on the component properties was investigated. Grinding reduced the particle sizes and produced oxide-free particle surface areas, which were obtained by the silane-doped atmosphere. This allows the TiAl powder to be processed by die pressing and sintering. The oxide-free particle surface areas were verified by X-ray measurements. The bare surface areas increase the pressability, green strength, and hardness of the sintered parts. However, these properties deteriorate due to renewed oxidation. Grinding increases the density of the components and also reveals a finer structure in the microstructure. In the future, the changes in the powder caused by ball milling will be investigated in more detail. In particular, the mechanisms behind the oxide layer break-up and the resulting possibilities for process optimisation during sintering will be further investigated.

References

1. Liu, B.; Liu, Y.; Zhang, W.; Huang, J.S. Hot deformation behavior of TiAl alloys prepared by blended elemental powders. *Intermetallics* **2011**, *19*, 154–159. [CrossRef]
2. Clemens, H.; Mayer, S. Design, Processing, Microstructure, Properties, and Applications of Advanced Intermetallic TiAl Alloys. *Adv. Eng. Mater.* **2013**, *15*, 191–215. [CrossRef]

3. Clemens, H.; Mayer, S.; Heilmaier, M. Pulvermetallurgische Herstellung von innovativen Hochtemperaturwerkstoffen. *BHM Berg-Und Hüttenmännische Monatshefte* **2021**, *166*, 1–7. [CrossRef]

4. Voisin, T.; Monchoux, J.-P.; Durand, L.; Karnatak, N.; Thomas, M.; Couret, A. An Innovative Way to Produce γ-TiAl Blades: Spark Plasma Sintering. *Adv. Eng. Mater.* **2015**, *17*, 1408–1413. [CrossRef]

5. Bewlay, B.P.; Nag, S.; Suzuki, A.; Weimer, M.J. TiAl alloys in commercial aircraft engines. *Mater. High Temp.* **2016**, *33*, 549–559. [CrossRef]

6. Mogale, N.; Matizamhuka, W. Spark Plasma Sintering of Titanium Aluminides: A Progress Review on Processing, Structure-Property Relations, Alloy Development and Challenges. *Metals* **2020**, *10*, 1080. [CrossRef]

7. Beiss, P. *Pulvermetallurgische Fertigungstechnik*; Springer Vieweg: Berlin/Heidelberg, Germany, 2013. [CrossRef]

8. Kariya, S.; Issariyapat, A.; Bahador, A.; Umeda, J.; Shen, J.; Kondoh, K. Ductility improvement of high-strength Ti–O material upon heteromicrostructure formation. *Mater. Sci. Eng. A* **2022**, *842*, 143041. [CrossRef]

9. Groza, J.R.; Zavaliangos, A. Sintering activation by external electrical field. *Mater. Sci. Eng. A* **2000**, *287*, 171–177. [CrossRef]

10. Jiao, L.; Feng, Q.; He, S.; Duan, B.; Dou, Z.; Li, C.; Lu, X. Direct oxygen removal from titanium aluminide scraps by yttrium reduction. *Nonferrous Met. Soc. China* **2021**, *32*, 2428–2437. [CrossRef]

11. Behrens, B.-A.; Bonhage, M.; Bohr, D. Neuartige Verfahrenskombination zur Verarbeitung von Werkstoffen auf Titanaluminid-Basis unter sauerstofffreier Atmosphäre **2020**, *23*. Umformtechnisches Kolloquium Hannover, Aktuelle Entwicklungen im Bereich der Umformtechnik, ISBN: 978-3-95900-423-7. Available online: https://www.tewiss-verlag.de/katalog/details/?isbn=978-3-95900-423-7 (accessed on 6 July 2023).

12. Bakulin, A.V.; Hocker, S.; Kulkova, S.E. Role of Intermediate Metal and Oxide Layers in Change of Adhesion Properties of TiAl/Al$_2$O$_3$ Interface. *Phys. Mesomech.* **2021**, *24*, 523–532. [CrossRef]

13. Attia, M. Cold-isostatic pressing of metal powders: A review of the technology and recent developments. *Solid State Mater. Sci.* **2021**, *46*, 587–610. [CrossRef]

14. Bay, N. Mechanisms Producing Metallic Bonds in Cold Welding. *Weld. J.* **1983**, *62*, 137.

15. Pflumm, R.; Friedle, S.; Schütze, M. Oxidation protection of g-TiAl-based alloys e A review. *Intermetallics* **2014**, *56*, 1–14. [CrossRef]

16. Gökce, A.; Findik, F. Mechanical and physical properties of sintered aluminum powders. *J. Achievments Mater. Manuf. Eng.* **2008**, *30*, 157–164.

17. Mphahlele, M.R.; Olubambi, P.A.; Olevsky, E.A. Advances in Sintering of Titanium Aluminide: A Review. *JOM* **2023**, *75*, 2877–2896. [CrossRef]

18. Gerling, R.; Clemens, H.; Schimansky, F.P. Powder Metallurgical Processing of Intermetallic Gamma Titanium Aluminides. *Adv. Eng. Mater.* **2004**, *6*, 23–38. [CrossRef]

19. Meier, G.H.; Pettit, F.S.; Hu, S. Oxidation behavior of titanium aluminides. *J. Phys.* **1993**, *3*, 395–402. [CrossRef]

20. Diaz, M.R.; Szafarska, M.; Gustus, R.; Möhwald, K.; Maier, H.J. Oxide Free Wire Arc Sprayed Coatings—An Avenue to Enhanced Adhesive Tensile Strength. *Metals* **2022**, *12*, 684. [CrossRef]

21. Holländer, U.; Wulff, D.; Langohr, A.; Möhwald, K.; Maier, H.J. Brazing inSiH 4-Doped Inert Gases: A New Approach to an Environment Friendly Production Process. *Int. J. Precis. Eng. Manuf. Green Technol.* **2019**, *7*, 1059–1071. [CrossRef]

22. Murty, B.S.; Rao, M.M.; Ranganthan, S. Milling maps and amorphization during mechanical alloying. *Acta Metall. Mater.* **1994**, *43*, 2443–2450. [CrossRef]

23. Qu, S.; Li, X.; Li, Y.; Hu, L.; Erde, W. Manufacturing a TiAl alloy by high-energy ball milling and subsequent reactive sintering. *Rare Met.* **2006**, *25*, 21–26. [CrossRef]

24. Behrens, B.A.; Brunotte, K.; Peddinghaus, J.; Heymann, A. Influence of dwell time and pressure on SPS process with tita-2 nium aluminides. *Metals* **2021**, *12*, 83. [CrossRef]

25. Gustus, R.; Szafarska, M.; Maus-Friedrichs, W. Oxygen-free transport of samples in silane-doped inert gas atmospheres for surface analysis. *J. Vac. Sci. Technol. B* **2021**, *39*, 54204. [CrossRef]

26. Scofield, J.H. Hartree-Slater subshell photoionization cross-sections at 1254 and 1487 eV. *J. Electron Spectrosc. Relat. Phenom.* **1975**, *8*, 129–137. [CrossRef]

27. Reilman, R.F.; Msezane, A.; Manson, S.T. Relative intensities in photoelectron spectroscopy of atoms and molecules. *J. Electron Spectrosc. Relat. Phenom.* **1976**, *8*, 389–394. [CrossRef]

28. Heymann, A.; Peddinghaus, J.; Brunotte, K.; Behrens, B.-A. Investigations on the Consolidation of TNM Powder by Admixing Different Elemental Powders. In *Metal 2022, 31st International Conference on Metallurgy and Materials: Conference Proceedings*; Tanger: Ostrava, Czech Republic, 2022; pp. 639–644.

29. Zhang, P.; Li, S.X.; Zhang, Z.F. General relationship between strength and hardness. *Mater. Sci. Eng. A* **2011**, *529*, 62–73. [CrossRef]

30. *DIN EN ISO 6507*; Metallische Werkstoffe—Härteprüfung nach Vickers—Teil 1: Prüfverfahren. Beuth Verlag: Berlin, Germany, 2018.

31. Szafarska, M. Gas Phase Reaction of Silane with Water at Different Temperatures and Supported by Plasma. *ACS Omega* **2023**, *8*, 8388–8396. [CrossRef]

32. Maier, H.J.; Herbst, S.; Denkena, B.; Dittrich, M.A.; Schaper, F.; Worpenberg, S.; Gustus, R.; Maus-Friedrichs, W. Towards Dry Machining of Titanium-Based Alloys: A New Approach Using an Oxygen-Free Environment. *Metals* **2020**, *10*, 1161. [CrossRef]

33. Barienti, K.; Werwein, S.; Herbst, S.; Maier, H.J.; Nürnberger, F. A novel way to reduce the critical deformation for cold roll bonding. *Manuf. Lett.* **2023**, *36*, 9–12. [CrossRef]

34. Lee, P.A. Oxide formation on Fe and Ti thin films and on Fe thin films modified with ultrathin layers of Ti. *Surf. Interface Anal.* **1991**, *17*, 48–56. [CrossRef]

35. Wang, X.H.; Zhou, Y.C. Layered Machinable and Electrically Conductive Ti2AlC and Ti3AlC2 Ceramics: A Review. *J. Mater. Sci. Technol.* **2010**, *26*, 385–416. [CrossRef]

36. Tallman, D.J.; Anasori, B.; Barsoum, M.W. A Critical Review of the Oxidation of Ti_2AlC, Ti_3AlC_2 and Cr_2AlC in Air. *Mater. Res. Lett.* **2013**, *1*, 115–125. [CrossRef]